

## The Fe/O elemental abundance ratio in the solar wind as observed with SOHO CELIAS CTOF

M. R. Aellig,<sup>1,2</sup> S. Hefti,<sup>1</sup> H. Grünwaldt,<sup>3</sup> P. Bochsler,<sup>1</sup> P. Wurz,<sup>1</sup>  
F. M. Ipavich,<sup>4</sup> and D. Hovestadt<sup>5</sup>

**Abstract.** Using data of the Charge Time-of-Flight (CTOF) mass spectrometer of the Charge, Element, and Isotope Analysis System (CELIAS) on board the Solar and Heliospheric Observatory (SOHO) from  $\sim 80$  days of observation around solar minimum we derive a value for the Fe/O abundance ratio for the inecliptic solar wind of  $0.11 \pm 0.03$ . Since Fe has a low first ionization potential (FIP) and O is a high-FIP element, their relative abundance is diagnostic for the FIP fractionation process. The unprecedented time resolution of the CELIAS CTOF sensor allows a fine-scaled study of the Fe/O ratio as a function of the solar wind bulk speed. On average, the Fe/O abundance ratio shows a continuous decrease by a factor of 2 with increasing solar wind speed between 350 and 500 km/s. This corresponds to the well-known FIP effect dependence. Our value at  $\sim 500$  km/s agrees with the previously observed Fe/O ratio in the fast solar wind emerging from polar coronal holes whereas the value for speeds below 350 km/s is consistent with a remote abundance determination in the leg of a coronal streamer. The variability of the Fe/O abundance ratio is much larger in the slow than in the fast solar wind.

### 1. Introduction

It is observationally established that in the corona and in the solar wind, elements with first ionization potentials (FIP) below  $\sim 10$  eV are systematically enriched relative to the high-FIP elements compared to their relative photospheric abundances. As the FIP is the organizing parameter of this fractionation, it is generally believed that this fractionation takes place where the species considered are partially ionized, i.e., in the upper chromosphere and the lower transition region. It has been pointed out by *Geiss and Bochsler* [1986] that the fractionation pattern is even more evident when observed as a function of the first ionization time (FIT) rather than the FIP.

As for the kinetic properties of the solar wind there is a fundamental difference of the strength of that fractionation between the coronal-hole-associated fast solar wind and the interstream solar wind. While the relative enrichment (typically compared to oxygen) amounts

to  $\sim 4$  in the slow solar wind, it is only  $\sim 2$  or less in the fast solar wind. The regime of the fast solar wind originating from the large polar coronal holes could only be probed when the Ulysses mission made its first polar pass. *Geiss et al.* [1995] reported measurements of the solar wind Mg/O relative abundance, a proxy for the strength of the FIP fractionation, and the  $O^{6+}/O^{7+}$  freeze-in temperature which is a proxy for the coronal electron temperature. On the basis of a superposed epoch analysis of several crossings of the high-speed stream emerging from the southern coronal hole they found steep and simultaneous changes of both the strength of the FIP fractionation and the freeze-in temperatures in the daily averages of these quantities. *Geiss et al.* concluded that there is one sharp boundary between the source regions of the slow and fast solar wind in the corona and in the chromosphere.

Several models have been set up to explain the observationally evidenced FIP effect, but as *von Steiger* [1996] states, none of them is able to fully and self-consistently explain the FIP effect. In his review, *von Steiger* [1996] notes that most of the models rely on ion-neutral separation and assume the solar EUV radiation as the ionizing agent. Several separation mechanisms were proposed, and sometimes strong assumptions about the model geometry are required.

*Marsch et al.* [1995] put forth a model that has not very stringent assumptions regarding the geometry but still is able to reproduce the observed fractionation pattern quantitatively by doing the ion-neutral separation in a diffusion layer. Extending this diffusion model, *Pe-*

<sup>1</sup>Physikalisches Institut, Universität Bern, Bern.

<sup>2</sup>Now at Center for Space Research, Massachusetts Institute of Technology, Cambridge.

<sup>3</sup>Max-Planck-Institut für Aeronomie, Katlenburg-Lindau, Germany.

<sup>4</sup>Department of Physics and Astronomy and Institute for Physical Science and Technology, University of Maryland, College Park.

<sup>5</sup>Max-Planck-Institut für Extraterrestrische Physik, Garching, Germany.

Copyright 1999 by the American Geophysical Union.

Paper number 1999JA900309.

0148-0227/99/1999JA900309\$09.00

ter [1996] introduced a chromospheric mass flow speed, the magnitude of which determines the strength of the FIP fractionation. The larger this chromospheric mass flow speed is (compared to an ionization-diffusion speed characteristic for each element), the shorter the separation process can act on the species, thus reducing the fractionation strength. We will take advantage of the quantitative predictions of this model by linking the chromospheric flow speed to the solar wind speed to compare this theory with our data.

Recently, Schwadron *et al.* [1999] explained the FIP fractionation in the slow solar wind by wave heating in coronal loops. Thus ions have larger scale heights than neutrals. Especially, in the upper chromosphere and the low transition region this effect is more pronounced for the low-FIP elements than for the high-FIP elements, leading to a relative enhancement of the low-FIP elements in the region of the loop above the transition region. The fractionated material is then released upon reconnection to eventually form the slow solar wind.

In this paper we will present determinations of the FIP fractionation in the interstream solar wind with very high time resolution with the CELIAS CTOF sensor on the SOHO mission. Whereas for the steady fast solar wind a good time resolution is not that important, it is crucial for the understanding of the FIP fractionation in the much more variable slow solar wind.

We will investigate the abundance of iron, a typical low-FIP (and low-FIT) element, relative to oxygen, a high-FIP (and high-FIT) element, in different solar wind speed regimes rather than considering only long-term averages. After a short description of the CELIAS CTOF sensor and the data analysis we will present the results in section 4. Both the overall properties of the Fe/O abundance ratio as well as some special time intervals are then discussed in section 5.

## 2. Instrument

The CTOF sensor of the SOHO CELIAS experiment is a linear time-of-flight (TOF) mass spectrometer. It combines an electrostatic analyzer, a TOF measurement, and a determination of the residual energy at the end of the TOF path. From these three measurements the energy, the mass, and the mass per charge of every ion detected can be derived unambiguously. To achieve a sufficient mass per charge resolution and to trigger the solid state detector efficiently, a postacceleration voltage is applied between the electrostatic analyzer and the TOF path. A more detailed description of the sensor is given by Hovestadt *et al.* [1995].

Since the sensor was not calibrated with iron ions, a model is used to extrapolate from the calibrated efficiencies of oxygen and argon to the efficiency of iron. While the entire instrument was modeled, we present here only one element of the instrument response model, i.e., the so-called double-coincidence-rate (DCR) efficiency, which will be referred to as “efficiency” in the following.

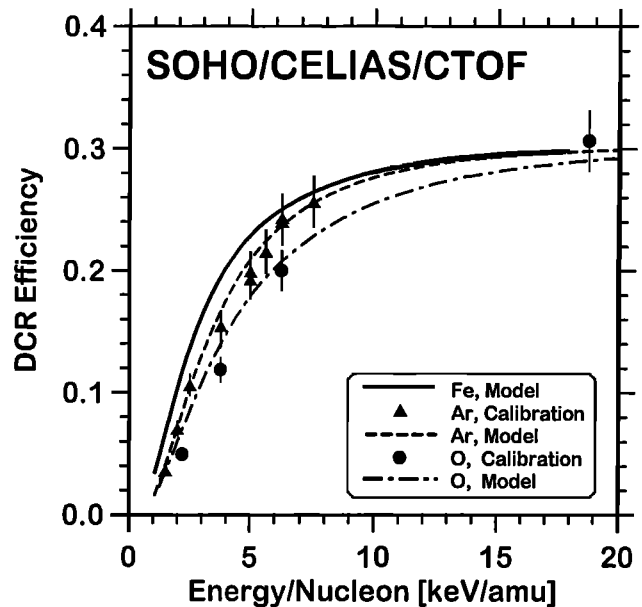


**Figure 1.** The double-coincidence-rate (DCR) efficiency as a function of the energy per nucleon. Calibration data (H. Grünwaldt, personal communication, 1998) are shown for argon (triangles) and oxygen (circles). The agreement between the calibration data and the modeled efficiencies for argon (dashed line) and oxygen (dash-dotted line) substantiate the modeled efficiency for iron (solid line).

This is the probability that the TOF of an ion entering the TOF section is measured. This efficiency is not the only one that influences the overall response of the sensor, but we concentrate on the DCR efficiency because it is the most crucial one to model for the analysis of variations of the relative abundance of different elements. Our efficiency model includes the production of secondary electrons at the carbon foil and at the solid state detector, the scattering of the ions in the carbon foil, the geometric transmission of the multiple grids, and the microchannel plate efficiencies. A detailed description of the entire instrument response model is given by Aellig [1998]. Figure 1 shows the calibrated and modeled efficiencies for oxygen and argon and the modeled efficiencies of iron. The good agreement between our model and the calibration curves for both oxygen and argon substantiates the extrapolation of our model to noncalibrated species such as iron. We estimate the relative uncertainty of the double-coincidence-rate efficiency for iron to be of the order of 10% in the energy range typical for solar wind iron ions after postacceleration within the sensor.

## 3. Data Analysis

The densities of the different iron charge states have been derived on the basis of an instrument response model together with a maximum likelihood inversion algorithm [Aellig, 1998; Aellig *et al.*, 1998]. The densities of the oxygen ions have been determined by Hefti

[1997]. The total iron density is derived from the charge states  $\text{Fe}^{7+}$  to  $\text{Fe}^{16+}$ , which covers more than 95% of all iron species during non-coronal-mass-ejection (non-CME) periods. Lower charged iron ions have upper limits of 1% or even lower [Geiss *et al.*, 1992]. The total oxygen density is estimated from the sum of the densities of  $\text{O}^{6+}$  and  $\text{O}^{7+}$ . This is appropriate except for time periods of very high freeze-in temperatures  $T_{\text{O}76}$  (derived from the relative density of  $\text{O}^{6+}$  and  $\text{O}^{7+}$ ) of  $2 \times 10^6$  K, where the fraction of  $\text{O}^{8+}$  is  $\sim 7\%$  on the basis of the assumption of ionization equilibrium [Arnaud and Rothenflug, 1985].

The time interval of observation ranges from day of year (DOY) 150, 1996, to DOY 229, 1996. During this period of low solar activity the solar wind proton speed derived from SOHO CELIAS Proton Monitor (PM) data [Hefti, 1997; Ipavich *et al.*, 1998] ranged from 295 km/s to 580 km/s with a mean value of 385 km/s. The sample standard deviation for this period is 51 km/s. Four intervals with proton speeds in excess of 500 km/s are identified during the period observed. No CME was observed during this interval on the Sun-Earth line.

#### 4. Results

On the basis of the methods described in section 3, ion fluxes were determined for the time interval indicated. The ratio of the integrated fluxes of iron and of oxygen is determined to be  $0.11 \pm 0.03$  for the entire time period. The rather large uncertainty of this ratio is mainly caused by the conservatively estimated uncertainties of the instrumental efficiencies. Further recalibration of the spare model of the CELIAS CTOF sensor is expected to reduce the overall uncertainty. Figure 2 displays the correlation between the iron flux and the oxygen flux in the solar wind. It is seen from Figure 2 that the Fe/O abundance ratio increases for increasing fluxes. Indeed, a linear fit of the logarithm of the iron flux with the logarithm of the oxygen flux yields a slope which is significantly greater than 1. The latter would correspond to a constant abundance ratio of Fe/O over the flux range observed. In cases of high iron and oxygen fluxes, iron is on average more abundant relative to oxygen as compared to the long-term average of 0.11.

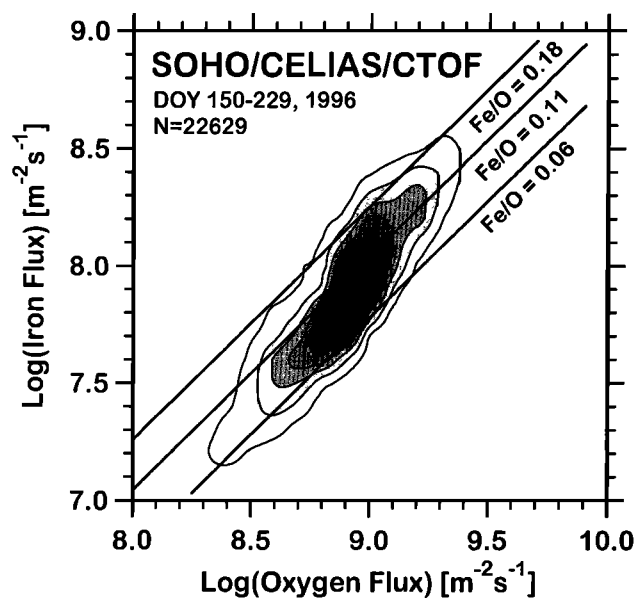


**Figure 2.** Correlation of the iron flux and the oxygen flux in the solar wind. The three solid lines represent cases of a constant flux ratio of Fe/O of 0.06, 0.11, and 0.18, respectively. The Fe/O ratio is not constant in all solar wind regimes and increases with increasing flux of oxygen. Data were taken between day of year (DOY) 150, 1996, and DOY 229.  $N$  denotes the number of spectra processed.

The linear correlation coefficient is 0.87. To assess a possible speed dependence of the Fe/O ratio, the speed range observed was first divided into three bins. The lowest bin contains speed values of  $< 360$  km/s, the highest bin contains speed values  $> 500$  km/s, and the center bin contains all speed measurements between these limits. Table 1 summarizes parameters of the distribution of the logarithms of Fe/O within these bins and for the entire data set. We consider the logarithms of the ratios because of their robustness with respect to extreme cases and because abundance ratios are approximately lognormally distributed [Bochsler, 1984]. Long-term averages of Fe/O and the values quoted from the literature are given linearly in this paper. The parameters given in Table 1 were calculated from the unweighted values of  $\log(\text{Fe}/\text{O})$ . Therefore the average value for the

**Table 1.** Mean and Standard Deviation  $s_{\log(\text{Fe}/\text{O})}$  of the Distributions of  $\log(\text{Fe}/\text{O})$  for Different Ranges of the Solar Wind Speed  $v_{sw}$

Speed, km/s	$\overline{\log(\text{Fe}/\text{O})}$	$s_{\log(\text{Fe}/\text{O})}$	$10^{\overline{\log(\text{Fe}/\text{O})}}$	Number of Cases
$295 < v_{sw} < 360$	-0.94	0.17	0.116	7053
$360 \leq v_{sw} \leq 500$	-1.04	0.15	0.091	14777
$500 \leq v_{sw} < 580$	-1.21	0.06	0.062	782
Entire range	-1.02	0.17	0.095	22612

The parameters were derived without weighting  $\log(\text{Fe}/\text{O})$  with the flux. For convenience,  $\overline{\log(\text{Fe}/\text{O})}$  is translated back into a linear ratio.

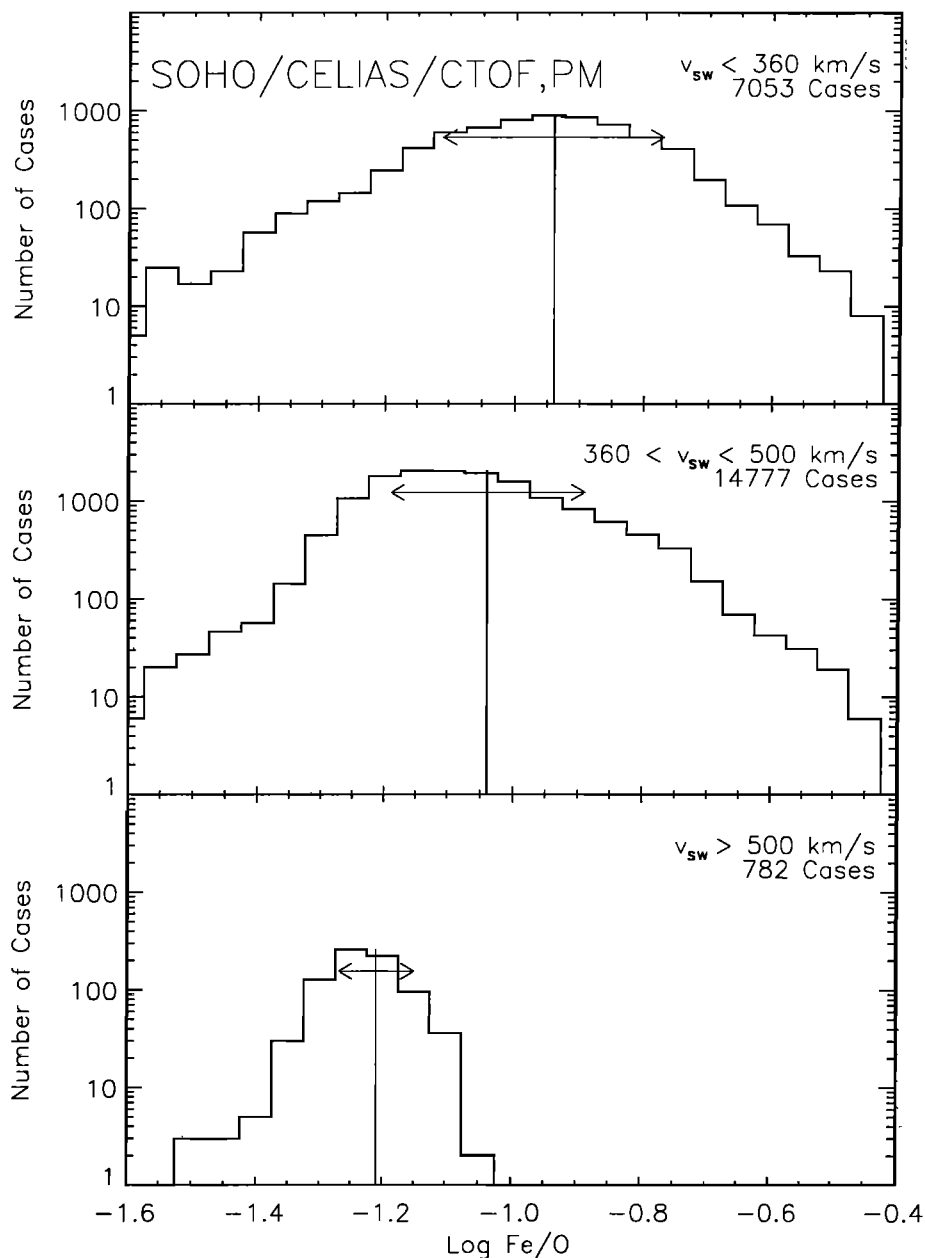


**Figure 3.** Histograms of  $\log \text{Fe}/\text{O}$  for three different ranges of the solar wind speed  $v_{sw}$ . In each histogram the vertical line indicates the mean value, and the horizontal arrows give the standard deviation of the sample. The cases in the highest speed range were accumulated during four distinct periods which are separated at least by 10 days.

entire speed range quoted in Table 1 differs from the value of 0.11 that is based on the ratio of the integrated fluxes of both species. The histograms of  $\log(\text{Fe}/\text{O})$  for the three different speed ranges are shown in Figure 3. From Table 1 as well as from Figure 3 it is obvious that the Fe/O ratio is decreasing with increasing solar wind speed. Furthermore, the variability of this ratio decreases with increasing wind speed. During four time intervals separated by at least 10 days, solar wind speeds above 500 km/s were observed. Thus it is unlikely that a selection effect could cause the small variability of  $\log(\text{Fe}/\text{O})$  in this speed range.

To better assess the speed dependence of  $\log(\text{Fe}/\text{O})$ , a finer binning of the solar wind speed was chosen. In Figure 4 the average values of  $\log(\text{Fe}/\text{O})$  are shown for speed intervals of 10 km/s width. The bars indicate the standard deviation of  $\log(\text{Fe}/\text{O})$  within each bin and thus measure the variability of  $\log(\text{Fe}/\text{O})$  in a narrow speed range. There is a continuous decrease of the averaged value of  $\log(\text{Fe}/\text{O})$  for increasing speed rather than a sharp distinction between two regimes. The following picture emerges from the data presented in Figure 4: At very low speed, i.e., below  $\sim 350$  km/s, the averages of  $\log(\text{Fe}/\text{O})$  in each speed bin seem to be compatible

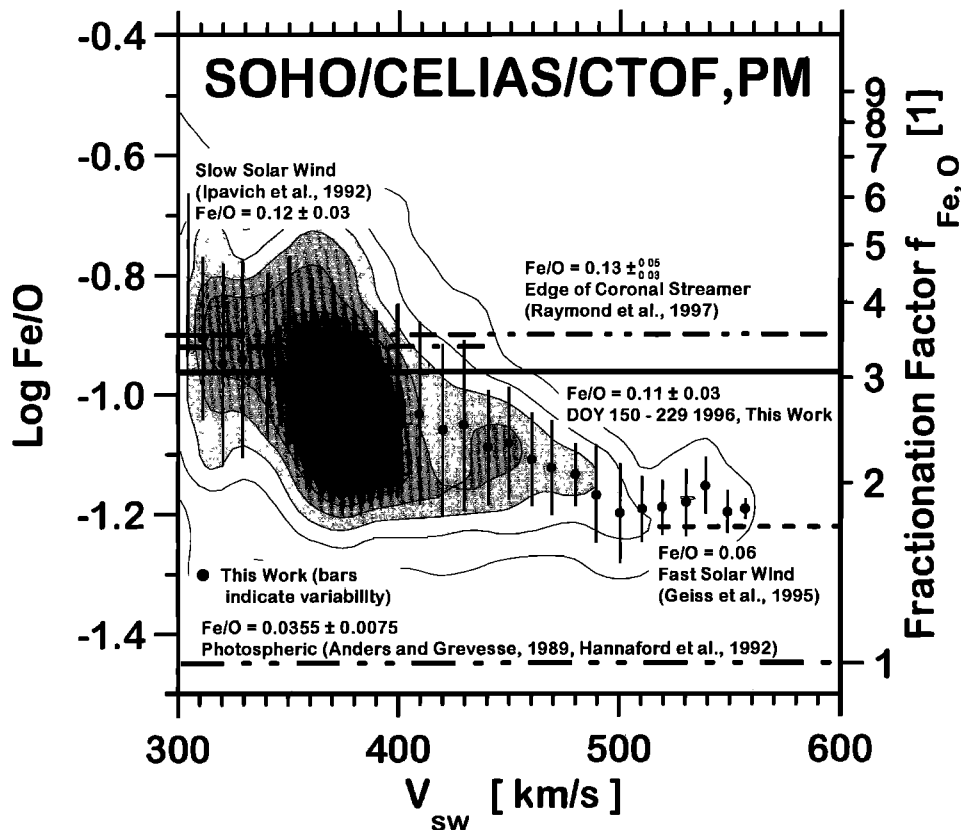


**Figure 4.** Contour plot (linearly spaced) of  $\log(\text{Fe}/\text{O})$  and the solar wind speed  $v_{sw}$  for the entire time period analyzed. The average values of  $\log(\text{Fe}/\text{O})$  within speed bins 10 km/s wide are plotted (dots) together with error bars that indicate the standard deviation of  $\log(\text{Fe}/\text{O})$  in the corresponding bin. For comparison, solar wind in situ measurements of  $\text{Fe}/\text{O}$  [Geiss et al., 1995; Ipavich et al., 1992], a remote determination of  $\text{Fe}/\text{O}$  at the edge of a coronal streamer [Raymond et al., 1997], and the photospheric abundance [Anders and Grevesse, 1989; Hannaford et al., 1992] are shown as well.

with a constant value of about -0.93. In the intermediate speed range between 350 and  $\sim 500$  km/s,  $\log(\text{Fe}/\text{O})$  decreases monotonically to a value of approximately -1.19. Above 500 km/s the average value of  $\log \text{Fe}/\text{O}$  seems to be constant at this level. The observed decrease is not caused by the organization of the data, as we illustrate with the following argument. If the smooth dependence observed was caused by the combination of coronal-hole-type solar wind with low  $\text{Fe}/\text{O}$  and comparably low speed and by solar wind with high  $\text{Fe}/\text{O}$  and comparably high speeds, the observed variability in the intermediate speed range between the two plateaus would be expected to increase with increasing speed, which is not the case.

Another way to organize the relative abundances of iron and oxygen is to plot them against a freeze-in temperature such as  $T_{\text{O}76}$ , which is derived from the relative density of  $\text{O}^{7+}$  and  $\text{O}^{6+}$  ions, as is done in Figure 5. In this representation there are two distinct regimes. For  $T_{\text{O}76}$  lower than  $\sim 1.4 \times 10^6$  K,  $\log(\text{Fe}/\text{O})$  is about -1.19 with quite a low variability. Above freeze-in temperatures of  $1.4 \times 10^6$  K there is, on average, a slight increase

of  $\log \text{Fe}/\text{O}$  from -1.01 to -0.91 with increasing freeze-in temperature.

After the presentation of the overall properties of the  $\text{Fe}/\text{O}$  ratio within the period of observation we consider special cases. In Figure 6, three selected time intervals of two days' duration are shown in detail. Large variations in the elemental abundance  $\text{Fe}/\text{O}$  are observed in the investigated period of slow solar wind ( $310 < v_{sw} < 370$  km/s) that seemingly are not correlated with the proton speed. There is no evident correlation seen between the fluctuations of  $\text{Fe}/\text{O}$  and the freeze-in temperature either. This period illustrates the large variability of the slow solar wind, e.g., with the  $\text{Fe}/\text{O}$  ratio changing by a factor of 4 between the end of day 154 and day 155, 0500 UT. The second case inspected is a transition from slow solar wind at  $\sim 400$  km/s on DOY 227, 1000 UT, to fast wind with a maximum speed of  $\sim 500$  km/s on DOY 227, 2000 UT. The  $\text{Fe}/\text{O}$  elemental abundance decreases from a value typical for the slow wind to a level characteristic for coronal hole solar wind between DOY 227, 1200 UT, and DOY 227, 1800 UT. On the same timescale, but  $\sim 2$  hours earlier, the oxy-

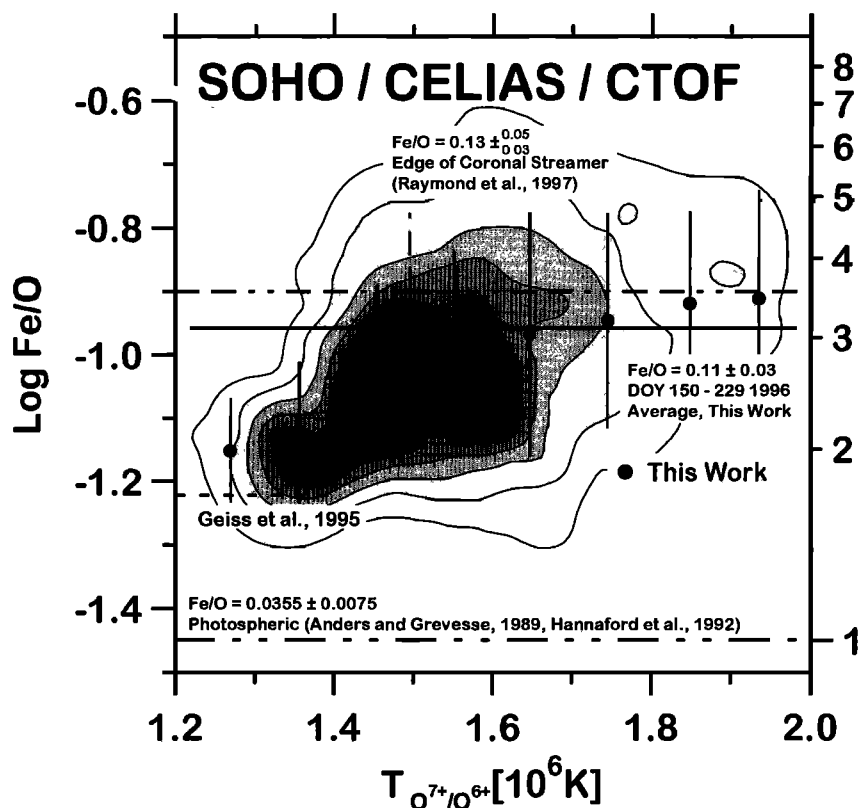


**Figure 5.** Contour plot of  $\log(\text{Fe}/\text{O})$  and the oxygen freeze-in temperature  $T_{\text{O}76}$ . The averages of  $\log(\text{Fe}/\text{O})$  for bins of  $T_{\text{O}76}$  of width  $10^5$  K (dots) are given. The error bars indicate the standard deviation of  $\log(\text{Fe}/\text{O})$  within the corresponding bin of the freeze-in temperature. For comparison, solar wind in situ measurements of  $\text{Fe}/\text{O}$  [Geiss *et al.*, 1995] in coronal-hole-type solar wind, a remote determination of  $\text{Fe}/\text{O}$  at the edge of a coronal streamer [Raymond *et al.*, 1997], and the photospheric abundance [Anders and Grevesse, 1989; Hannaford *et al.*, 1992] are shown as well.

gen freeze-in temperature decreases from  $1.8 \times 10^6$  K to  $< 1.4 \times 10^6$  K. The offset of 2 hours between the changes of the elemental abundance and the freeze-in temperature is shorter than the timescale of 6 hours on which they take place. In this case, the definition of the beginning and the end of the changes is somewhat arbitrary. The transition between the two speed regimes takes place on a timescale of  $\sim 8$  hours. The third case investigated is the beginning of a high-speed stream with proton speeds up to 580 km/s, which exhibits the properties of a coronal hole. Indeed, Hefti *et al.* [1999] showed, by backmapping of the solar wind onto the solar surface, that this high-speed stream emanates from an equatorial coronal hole that became known as elephant's trunk one solar rotation later. The freeze-in temperature steeply decreases in two steps between 0500 and 0700 UT on DOY 213 during the period of increasing solar wind speed. The  $\text{Fe}/\text{O}$  ratio is reduced by a factor of  $\sim 2$  on DOY 213, 0100 UT, within about half an hour. This very fast change of the elemental composition, however, precedes the signature given by the freeze-in temperature and the proton speed by  $\sim 5$  hours. During this period (shaded area)

an  $\text{Fe}/\text{O}$  ratio typical for fast solar wind is observed simultaneously with freeze-in temperatures and proton speeds characteristic of the slow wind. The timescale of the change of the solar wind speed on the leading edge is  $\sim 4$  hours, and the change of the freeze-in temperature and the composition take place on even shorter timescales. The trailing edge (not shown) of the high-speed stream is seen in all three quantities simultaneously with smaller gradients than at the leading edge. A closer view of the interesting time period of low  $\text{Fe}/\text{O}$  and high freeze-in temperature around the change in speed on DOY 213 is shown in Figure 7 together with the proton speed, the proton thermal speed, the proton density, the N/S flow angle of the solar wind, and the He/H abundance ratio. While the proton parameters were derived from SOHO CELIAS PM data, the He/H abundance was derived from Wind high-resolution mass spectrometer (MASS) data and then shifted by a time lag derived from the radial separation of Wind and SOHO and from the solar wind speed. The proton density shows a smooth decrease prior to the steep decrease of the  $\text{Fe}/\text{O}$  abundance ratio. Furthermore, the N/S flow angle smoothly changes from positive to negative

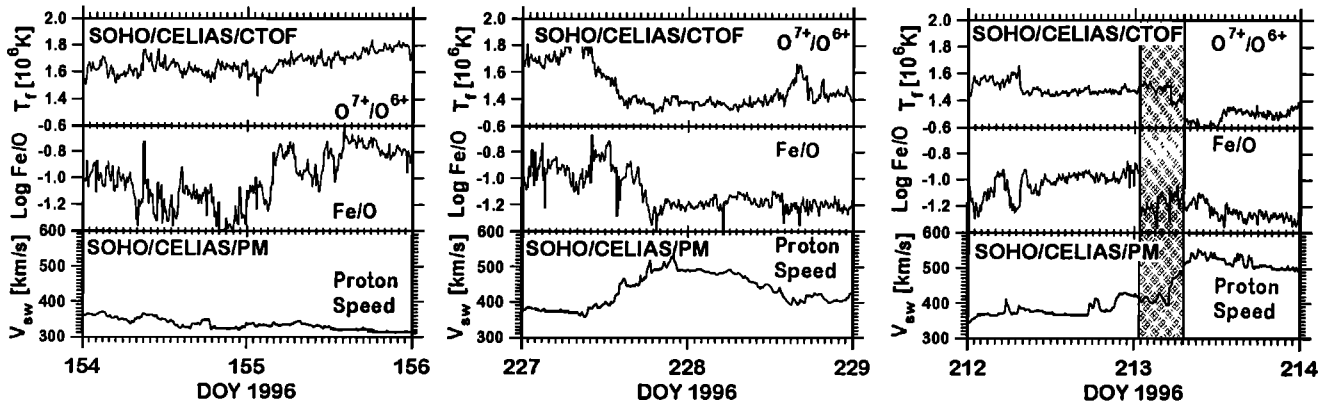


**Figure 6.** The Fe/O abundance in different solar wind regimes (middle graph in each frame). In the lower graph of each frame the solar wind speed  $v_{sw}$  is given and the freeze-in temperature  $T_f$  derived from the ion pair  $O^{7+}/O^{6+}$  is shown in the top graph of each frame. (left) Slow solar wind regime. (center) Solar wind speed increase from  $\sim 400$  km/s to  $\sim 500$  km/s. (right) Transition from slow to fast solar wind. The shaded region indicates the period of a low Fe/O ratio typical for coronal-hole-type solar wind and high freeze-in temperature characteristic for the low-speed solar wind.

values at the same time, while no obvious signature is visible either in the bulk or in the thermal speed of the protons. The He/H abundance ratio, extrapolated from Wind, starts to smoothly increase around the time of the jump of the Fe/O ratio. At DOY 213, 0515 UT, the freeze-in temperature  $T_{O76}$  decreases from  $1.5 \times 10^6$  K to  $\sim 1.4 \times 10^6$  K. At the same time, both the bulk and thermal speed of the protons increase, and the N/S flow angle changes from negative to positive values. Around this time, the He/H abundance increases to  $\sim 8\%$ . At DOY 213, 0715 UT, the freeze-in temperature  $T_{O76}$  decreases steeply again from  $1.4 \times 10^6$  K to  $\sim 1.25 \times 10^6$  K. No obvious signature is seen in the other particle-related parameters shown in Figure 7. We analyzed also the magnetic field data (Wind Magnetic Field Investigation key parameter data) that were extrapolated from Wind to the location of SOHO using a procedure described by Aellig [1998]. These data, however, did not allow us to clearly classify this interesting event.

## 5. Discussion

Our flux weighted average for Fe/O of  $0.11 \pm 0.03$  is consistent with the value reported by Ipavich *et al.* [1992] for the inecliptic solar wind during a period of high solar activity and is, though considerably lower, also marginally consistent with the best estimate of  $0.19 \pm 0.07$  derived from the He/Fe abundance ratio reported by Schmid *et al.* [1988] for the previous solar maximum. A He/O abundance ratio of 75 [Bochsler *et al.*, 1986] was used to derive the Fe/O value from the He/Fe ratio. As Schmid *et al.* [1988] anticipated, there might have been a slight selection effect in their analysis which discriminated periods of low fluxes which are characterized, generally, by a lower Fe/O ratio as is seen from Figure 2. Compared to the photospheric

abundance relative to oxygen, iron is enriched in the slow solar wind by a factor of  $\sim 3$  which is typical for low-FIP elements. We calculate the photospheric abundance ratio of Fe/O from the iron abundance given by Hannaford *et al.* [1992] and the oxygen abundance given by Anders and Grevesse [1989]. The photospheric iron abundance of Hannaford *et al.* [1992] agrees with a previous determination reported by Holweger *et al.* [1990].

We assess the speed dependence of  $\log Fe/O$  with the averaged values of  $\log Fe/O$  over narrow speed bins. Below proton speeds of 350 km/s we find the bin averages of  $\log Fe/O$  to be compatible with a constant value corresponding to a ratio Fe/O of 0.12. This number is derived from the mean of the bin averages. For proton speeds above 500 km/s the  $\log Fe/O$  value also seems to be independent of the wind speed. In this speed range we determine the ratio Fe/O to be  $\sim 0.06$  in the same manner as before. This value agrees with the value reported by Geiss *et al.* [1995] for coronal-hole-type solar wind and indicates that the solar wind we observed at speeds in excess of 500 km/s emanated either from an equatorial coronal hole or an equatorial extension of a polar coronal hole. The plateaus of speed-independent Fe/O values are separated by the well-known factor of 2 by which, on average, the strength of the FIP fractionation effect varies between the different regimes of the solar wind. What is new, to our knowledge, is the observation of an intermediate regime of FIP fractionation strength in the intermediate range of solar wind speeds between 350 and 500 km/s. On average, a smooth and continuous change between the plateaus outside this speed interval is observed. Furthermore, the variability decreases as the speed increases.

A FIP fractionation model by Peter [1996] which assumes full stationarity of the chromosphere predicts the

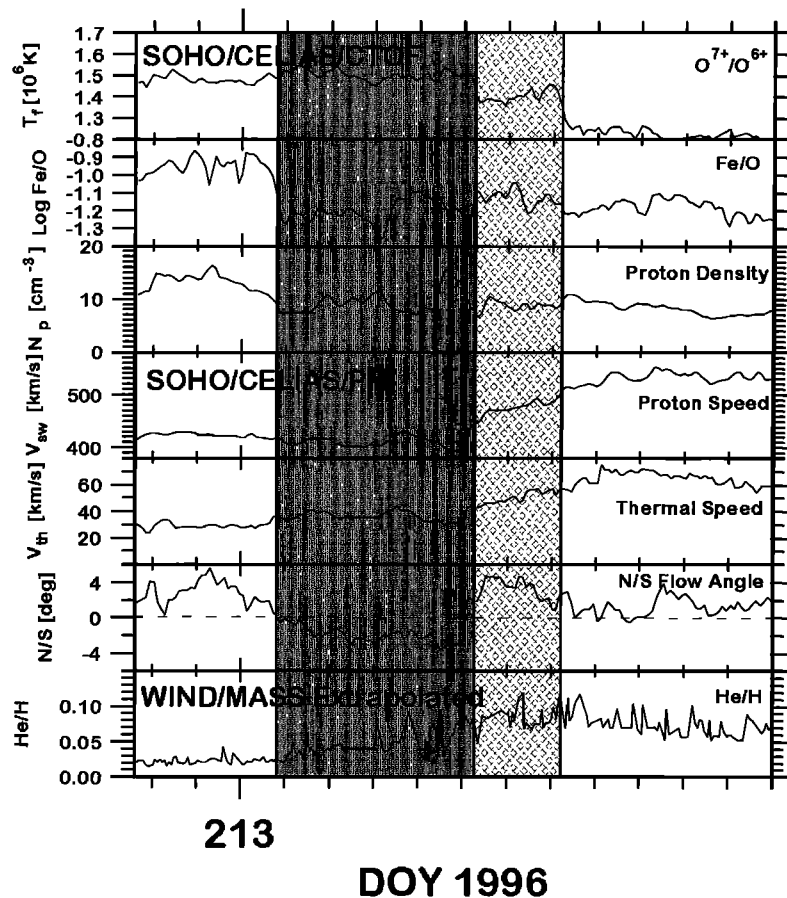


**Figure 7.** The freeze-in temperature  $T_{O76}$ , the Fe/O abundance, the density  $N_p$ , bulk speed, thermal speed  $v_{th}$ , and the N/S flow angle of the protons during the speed increase shown in Figure 6 (right frame). Extrapolated from measurements at Wind, the He/H abundance is given as well. The dark shading corresponds to the time interval of 4.5 hours between the steep decrease of the Fe/O abundance ratio and the steep decrease of the freeze-in temperature  $T_{O76}$  from  $1.5 \times 10^6$  K to  $\sim 1.4 \times 10^6$  K. The hatched region is the time interval of 2 hours between the jump of  $T_{O76}$  just mentioned and the second step decrease from  $1.4 \times 10^6$  K to  $\sim 1.25 \times 10^6$  K. One tick mark on the  $x$  axis corresponds to 1 hour.

fractionation strength to vary with the chromospheric mass flow speed  $U_H$  according to

$$f_{\text{Fe,O}} = \frac{1 + \sqrt{1 + 4(w_{\text{Fe}}/U_H)^2}}{1 + \sqrt{1 + 4(w_{\text{O}}/U_H)^2}}, \quad (1)$$

where  $w_{\text{Fe}}$  and  $w_{\text{O}}$  denote the ionization-diffusion speeds of iron and oxygen, respectively. The model assumes diffusion across a horizontal layer as the separation mechanism. As in the analytic model by Marsch *et al.* [1995], the ionization-diffusion speed is the governing parameter since it is influenced both by the first ionization time and the diffusion coefficient in the layer. Species with short ionization times and large diffusion coefficients are favored. Additionally, in the model by Peter [1996] an upward flow speed  $U_H$  reduces the time spent in the fractionating diffusion layer, therefore reducing the strength of the fractionation.

Assuming a chromospheric density of  $4 \times 10^{16} \text{ cm}^{-3}$  and a temperature of  $10^4$  K, the speeds  $w_{\text{Fe}}$  and  $w_{\text{O}}$  were

calculated to be 0.63 km/s and 0.11 km/s according to Marsch *et al.* [1995]. For these chromospheric conditions the fractionation factors  $f_{\text{Fe,O}}$  derived from the data were used to calculate the chromospheric mass flow speeds  $U_H$  that, in this model, account for the observed fractionation. This was done by inverting (1). The fractionation factors  $f_{\text{Fe,O}}$  for the entire period of observation were calculated from the observed Fe/O ratio in the solar wind, adopting a photospheric Fe/O ratio of  $0.0355 \pm 0.0025$  [Anders and Grevesse, 1989; Hannaford *et al.*, 1992]. A contour plot of the measured solar wind speeds  $v_{sw}$  at 1 AU and the mass flow speeds  $U_H$  derived from the fractionation factors is shown in Figure 8. On average, an increase of the mass flow speed  $U_H$  is seen with increasing solar wind speed. Corresponding to the plateau of the Fe/O ratios for solar wind speeds above 500 km/s, the mass flow speeds level off at the same solar wind speed. The contour plot indicates that there is an upper limit of  $U_H$  of  $\sim 0.6$  km/s. The absolute value of this upper limit, however, depends upon the



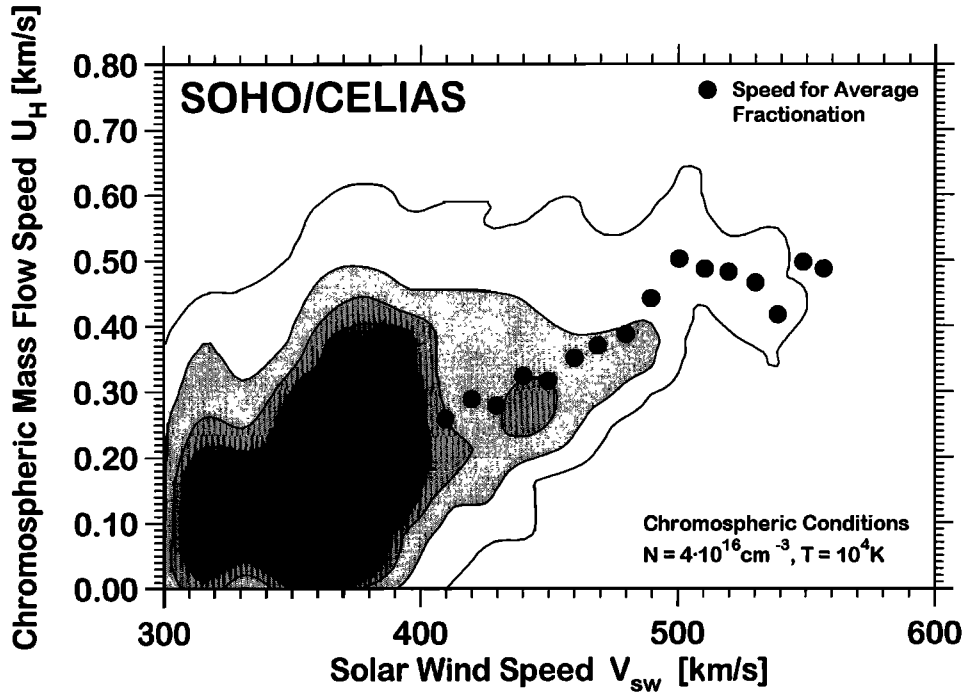


Figure 8. Contour plot (linearly spaced) of the chromospheric mass flow speed  $U_H$  and the solar wind bulk speed  $v_{sw}$  for the entire time period analyzed. The speed  $U_H$  was derived from the observed fractionation factors  $f_{\text{Fe},\text{O}}$  using (1). Correspondingly, from the average values of  $\log(\text{Fe}/\text{O})$  within speed bins 10 km/s wide, average values of  $U_H$  for the same bins of the solar wind speed were derived (dots).

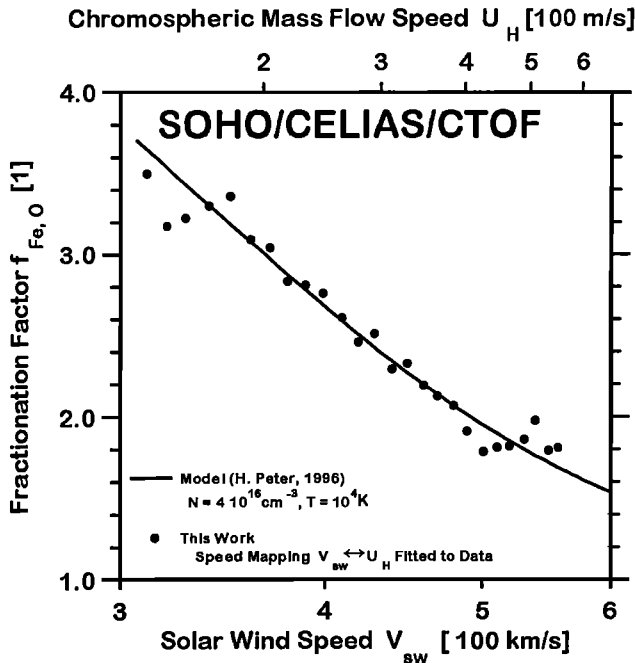
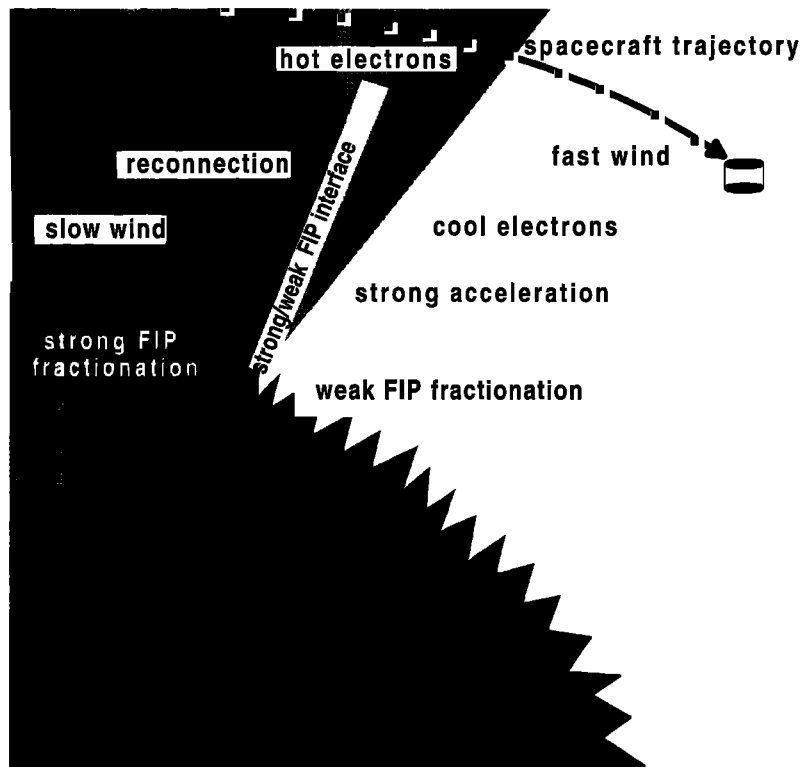


Figure 9. Speed dependence of the fractionation factor  $f_{\text{Fe},\text{O}}$ . The modeled fractionation (solid line) depends on the chromospheric mass flow speed  $U_H$  (top axis) according to (1). The mapping between  $U_H$  and the solar wind proton speed  $v_{sw}$  (equation (2)) was fitted to match the average fractionation factors derived from the data (dots).

assumed density and temperature in the chromosphere. A change in the chromospheric density by a factor of 4 changes this limit by  $< 50\%$ . Note that the model by Peter [1996] in (1) cannot explain fractionation factors larger than  $\sim 6$ , i.e., cases of Fe/O greater than 0.21. Those cases are not visible in Figure 8. We fitted the averages of the derived mass flow speeds over the range of observed solar wind speeds with the power law relation

$$\log v_{sw} = 2.85 + 0.41 \log U_H \quad (2)$$

We achieve a good agreement between the observed fractionation and the predicted fractionation (1), as is seen from Figure 9. We note that the model, though it assumes stationarity, may explain the averaged fractionation well. For this discussion we assume that the fractionation solely takes place in the upper chromosphere and that the material is supplied from there with virtually no elemental fractionation into the solar wind. It is important to note that the agreement shown in Figure 9 is the result of the mapping between the parameter relevant to the fractionation strength, the chromospheric mass flow speed  $U_H$ , and the solar wind speed  $v_{sw}$ . Other models should also be able to account for the observed smooth decrease of the fractionation strength with the solar wind speed if the parameters relevant to the fractionation are tied to the solar wind speed. For example, for the model by Schwadron *et al.*, [1999] this could be the wave-particle interaction rate.



**Figure 10.** Sketch of a possible situation as encountered during the period covered in the right-most frame of Figure 6. The spacecraft, which is moving relative to the (anticlockwise) rotating Sun, leaves the region above the equatorial streamer belt and crosses first the boundary of low-FIP fractionation associated with the precursor of the “elephant trunk” extension of the northern coronal hole. It remains for a few hours in the solar wind which emanates from a relatively hot corona before it finally travels into the fully coronal-hole-dominated solar wind regime. A possible reason for hot electrons expanding over the low/high FIP interface is magnetic reconnection and associated heating of electrons and ions extending somewhat into the high-speed regime.

Recently, measurements of elemental abundances in coronal streamers have been performed with the SOHO Ultraviolet Coronagraph Spectrometer [Raymond *et al.*, 1997]. From their results we derive a Fe/O ratio of  $0.13 \pm 0.05$  for the leg of an equatorial coronal streamer. Raymond *et al.* address the edge of the streamer, bright in O VI, as “leg” (J. Raymond, personal communication, 1999). This value is consistent with our average value in the speed range below 350 km/s which indicates that very slow solar wind might emerge from the edge of equatorial coronal streamers. Though these structures are magnetically closed, plasma could stream away when the closed structures are opened from time to time by magnetic reconnection. On the basis of the model by Peter [1996] we expect the FIP fractionation to be strongest for magnetically closed regions since the upflow velocities there are smallest.

The analysis of selected time periods shown in Figure 6 confirms the close link between the corona and the chromosphere on short spatial scales. This link is discussed by Geiss *et al.* [1995] for the large-scale structures, i.e., for the transition between slow solar wind and the fast solar wind originating from the polar coro-

nal holes; we gave a short summary of Geiss *et al.*'s results in section 1. With the improved time resolution of the CELIAS CTOF sensor this is also seen in a special case (Figure 6, center frame) for a moderate increase of the solar wind speed. The Fe/O abundance ratio, a measure for the strength of the chromospheric elemental fractionation, and the freeze-in temperature, a proxy for the coronal electron temperature, change with a temporal offset which is shorter than the timescale of  $\sim 6$  hours over which the change takes place. This differs for another transition between the slow solar wind and coronal-hole-type solar wind (Figure 6, right frame) in which the changes are not simultaneous and are much faster. The change of the composition takes place in  $< 1$  hour whereas the change of the freeze-in temperature lasts  $\sim 2$  hours. More interestingly, there is a significant offset of  $\sim 6$  hours between the jumps of the composition and the oxygen freeze-in temperature. From the data presented we can neither conclusively classify this event nor explain this offset of 6 hours. In Figure 10 a possible scenario which could explain this observed behavior is schematically shown. Hot electrons typical for the coronal source region of the slow

wind might be produced on the low-FIP fractionation side of the low/high FIP interface because of magnetic reconnection taking place in the corona close to the interface.

Considerable variations of the Fe/O elemental abundance are observed within the very slow solar wind on short timescales of a few hours with no obvious related change of the freeze-in temperature or the solar wind speed (Figure 6, left frame). This demonstrates the filamentary structure of the slow solar wind. The large variations observed on short timescales are compatible with the picture of the slow solar wind being the result of very small coronal mass ejections (CME) that take place continuously, or of small but frequent reconnection events. These small-scale events are characterized by a wide range of observed Fe/O abundance ratios and freeze-in temperatures. This large variability of  $\log(\text{Fe}/\text{O})$  is observed for freeze-in temperatures  $T_{\text{O}76}$  greater than  $1.45 \times 10^6$  K as can be seen in Figure 5. Above this temperature there is, on average, only a slight dependence of  $\log(\text{Fe}/\text{O})$  upon the freeze-in temperature. Moreover, there is only a weak correlation between the Fe/O abundance ratio and the observed freeze-in temperature for periods of high freeze-in temperatures, i.e., for the slow solar wind.

## 6. Conclusions

A Fe/O flux ratio of  $0.11 \pm 0.03$  in the solar wind was determined from SOHO CELIAS CTOF data for an extended time period of 80 days, which is compatible with previous measurements. For solar wind speeds below 350 km/s our average values for Fe/O are independent of the speed  $v_{sw}$ . They are consistent with a remote determination of Fe/O in the leg of an equatorial coronal streamer, which provides evidence that the edges of equatorial streamers are the sources of the very slow solar wind. For solar wind speeds above 500 km/s the Fe/O ratio is, on average, independent of the wind speed. In this speed range we derive a ratio Fe/O of  $\sim 0.06$  which is consistent with measurements of Ulysses of the fast solar wind emerging from the polar coronal holes. In the intermediate speed range between 350 and 500 km/s we observe, on average, a linear decrease of  $\log(\text{Fe}/\text{O})$  with the solar wind speed  $v_{sw}$ . By the application of a model by Peter [1996] the observed speed dependence in the intermediate speed range could be explained if the chromospheric mass flow speed relevant to his elemental fractionation model relates to the solar wind speed via a power law with parameters fitted to our data.

Within the slow solar wind a high variability of the Fe/O abundance ratio is observed. Only a weak correlation between the Fe/O abundance and the freeze-in temperature is seen for the slow wind which is characterized by high freeze-in temperatures.

**Acknowledgments.** This work is supported by the Swiss National Science Foundation, by the PRODEX program of ESA, by DARA, Germany, under contracts 50 OC 89056 and 50 OC 96087, and by NASA, United States, under contract NAS-31166. CELIAS is a joint effort of five hardware institutions under the direction of the Max-Planck-Institut für extraterrestrische Physik (prelaunch) and the University of Bern (postlaunch). The Max-Planck-Institut für Aeronomie was the prime hardware institution for CTOF, the University of Bern provided the deflection system of CTOF, and the Technische Universität Braunschweig provided the DPU.

Janet G. Luhmann thanks Eberhard Möbius and Victor Hansteen for their assistance in evaluating this paper.

## References

- Aellig, M. R., Freeze-in temperatures and relative abundances of iron ions in the solar wind measured with SOHO/CELIAS/CTOF, Ph.D. thesis, Univ. of Bern, 1998.
- Aellig, M. R., et al., Iron freeze-in temperatures measured by SOHO/CELIAS/CTOF, *J. Geophys. Res.*, *103*, 17,215–17,222, 1998.
- Anders, E., and N. Grevesse, Abundances of the elements: Meteoritic and solar, *Geochim. Cosmochim. Acta*, *398*, 197–214, 1989.
- Arnaud, M., and R. Rothenflug, An updated evaluation of recombination and ionization rates, *Astron. Astrophys. Suppl. Ser.*, *60*, 425–470, 1985.
- Bochsler, P., Helium and oxygen in the solar wind: Dynamic properties and abundances of elements and helium isotopes as observed with the ISEE-3 Plasma Composition Instrument, Habilitationsschrift, Univ. of Bern, 1984.
- Bochsler, P., J. Geiss, and S. Kunz, Abundances of carbon, oxygen, and neon in the solar wind during the period from August 1978 to June 1982, *Sol. Phys.*, *103*, 177–201, 1986.
- Geiss, J., and P. Bochsler, Solar wind composition and what we expect to learn from out-of-ecliptic measurements, in *The Sun and Heliosphere in Three Dimensions*, edited by R. G. Marsden, pp. 173–186, D. Reidel, Norwell, Mass., 1986.
- Geiss, J., K.W. Ogilvie, R. von Steiger, U. Mall, G. Gloeckler, A.B. Galvin, F.M. Ipavich, B. Wilken, and F. Gliem, Ions with low charges in the solar wind as measured by SWICS on board Ulysses, in *Solar Wind Seven*, edited by E. Marsch and R. Schwenn, pp. 341–348, Pergamon, New York, 1992.
- Geiss, J., et al., The southern high-speed stream: Results from the SWICS instrument on Ulysses, *Science*, *268*, 1033–1036, 1995.
- Hannaford, P., R.M. Lowe, N. Grevesse, and A. Noels, Lifetimes of Fe II and the solar abundance of iron, *Astron. Astrophys.*, *259*, 301–306, 1992.
- Hefti, S., Solar wind freeze-in temperatures and fluxes measured with SOHO/CELIAS/CTOF and calibration of the CELIAS sensors, Ph.D. thesis, Univ. of Bern, 1997.
- Hefti, S., H. Grünwaldt, P. Bochsler, and M. R. Aellig, Oxygen freeze-in temperatures measured with SOHO CELIAS CTOF, *J. Geophys. Res.*, in press, 1999.
- Holweger, H., C. Heise, and M. Kock, The abundance of iron in the Sun derived from photospheric Fe II lines, *Astron. Astrophys.*, *232*, 510–515, 1990.
- Hovestadt, D., et al., CELIAS: The Charge, Element, and Isotope Analysis System for SOHO, *Sol. Phys.*, *162*, 441–481, 1995.
- Ipavich, F. M., A. B. Galvin, J. Geiss, K. W. Ogilvie,

- and F. Gliem, Solar wind iron and oxygen charge states and relative abundances measured by SWICS/Ulysses, in *Solar Wind Seven*, edited by E. Marsch and R. Schwenn, pp. 369–373, Pergamon, New York, 1992.
- Ipavich, F. M., et al., Solar wind measurements with SOHO: The CELIAS/MTOF proton monitor, *J. Geophys. Res.*, *103*, 17,205–17,214, 1998.
- Marsch, E., R. von Steiger, P. Bochsler, Element fractionation by diffusion in the solar chromosphere, *Astron. Astrophys.*, *301*, 261–276, 1995.
- Peter, H., Velocity-dependent fractionation in the solar chromosphere, *Astron. Astrophys.*, *312*, L37–L40, 1996.
- Raymond, J., et al., Composition of coronal streamers from the SOHO Ultraviolet Coronagraph Spectrometer, *Sol. Phys.*, *175*, 645–665, 1997.
- Schmid, J., P. Bochsler, and J. Geiss, Abundance of iron ions in the solar wind, *Astrophys. J.*, *329*, 956–966, 1988.
- Schwadron, N. A., L. A. Fisk, and T. H. Zurbuchen, Elemental fractionation in the slow solar wind, *Astrophys. J.*, *521*, 859–867, 1999.
- von Steiger, R., Solar wind composition and charge states, in *Solar Wind Eight*, edited by D. Winterhalter et al., pp. 193–198, AIP Press, Woodbury, New York, 1996.
- M. R. Aellig, Center for Space Research, Massachusetts Institute of Technology, Room 37-662B, 77 Massachusetts Avenue, Cambridge, MA 02139. (mra@space.mit.edu)
- P. Bochsler, S. Hefti, and P. Wurz, Physikalisches Institut, Universität Bern, Sidlerstrasse 5, CH-3012 Bern, Switzerland. (bochsler@soho.unibe.ch; hefti@soho.unibe.ch; wurz@soho.unibe.ch)
- H. Grünwaldt, Max-Planck-Institut für Aeronomie, D-37189 Katlenburg-Lindau, Germany. (gruenwaldt@linax1.dnet.gwdg.de)
- D. Hovestadt, Max-Planck-Institut für extraterrestrische Physik, D-85740, Garching, Germany.
- F. M. Ipavich, Department of Physics and Astronomy and IPST, University of Maryland, College Park, MD 20742. (ipavich@umdsp.dnet.nasa.gov)

(Received September 17, 1998; revised June 24, 1999; accepted June 24, 1999.)